

A dual-polarized multichroic antenna-coupled TES bolometer for terrestrial CMB Polarimetry

Roger O'Brient^a, Peter Ade^b, Kam Arnold^a, Jennifer Edwards^c, Greg Engargiola^d, William Holzapfel^a, Adrian T. Lee^{ae}, Xiao Fan Meng^f, Michael Myers^a, Erin Quealy^a, Gabriel Rebeiz^c, Paul Richards^a, Aritoki Suzuki^a

^aUniversity of California Berkeley Physics, Berkeley, CA 94720 USA;

^bSchool of Physics and Astronomy, Cardiff University, Cardiff, UK;

^cUniversity of California San Diego Electrical Engineering, La Jolla, CA 92092 USA;

^dUniversity of California Berkeley Radio Astronomy, Berkeley, CA 94720 USA;

^eSpace Sciences Laboratory, Berkeley, CA 94720 USA;

^fUniversity of California Berkeley Electrical Engineering, Berkeley, CA 94720 USA;

ABSTRACT

We are developing dual-polarized multi-channel antenna-coupled Transition Edge Sensor (TES) Bolometers for Cosmic Microwave Background (CMB) Polarimetry in terrestrial experiments. Each pixel of the array couples incident power into the lithographed microstrip circuits with a dual-polarized broadband planar sinuous antenna whose gain is increased with a contacting extended hemispherical lens. Microstrip filter manifolds partition the two-octave bandwidth into narrow channels before terminating at separate TES bolometers. We describe the design methodology and fabrication methods used, and also the results of optical tests that show high optical throughput in properly located bands, as well as high cross-polarization rejection. We have explored two antenna feeding schemes that result in different quality beams and we comment on the relative merits of each. Finally, we quantify the increases in mapping speed that an array of our multichroic pixels might realize over traditional monochromatic pixels.

Keywords: CMB Polarization, B-modes, Foreground Removal, Antenna-coupled TES Bolometers, Broadband Detectors, Sinuous Antenna, channelizer

1. INTRODUCTION

Physicists mapping the Cosmic Microwave Background (CMB) have made significant progress over the past two decades in characterizing its temperature and E-mode polarization anisotropies. They have used these data sets to constrain myriad cosmological parameters with unprecedented accuracy and hope to continue this trend with observations of B-mode anisotropies in the future.¹ B-mode maps could help constrain the sum of neutrino masses, the dark-energy equation of state,² and even the energy scale of inflation.³

Advancements in detector technology have made this success possible and current state-of-the-art bolometers provide background-noise-limited observations. As such, the only way to increase sensitivity is to increase throughput and several recent experiments have done this with large focal-plane arrays containing several hundred detectors.⁴

Typical focal planes contain pixels with 20-30% fractional bandwidth. This limited bandwidth is practical because terrestrial and balloon-bourn experiments must evade atmospheric lines whose high power can saturate detectors. Additionally, the CMB is contaminated with polarized galactic foregrounds in the form of thermal-dust and synchrotron emissions^{5,6}. Several up-coming experiments seek to characterize and remove these by mapping the sky at several frequency bands of finite width. Additionally, the atmospheric loading from water is stronger at shorter wavelengths and SuZIE-2 demonstrated that the high frequency channels can be used to control for atmospheric fluctuations to allow for background limited observations.⁷

Further author information: (Send correspondence to Roger O'Brient). E-mail: rogero@bolo.berkeley.edu
Color version available on line at: bolo.berkeley.edu/bolometers/publications.html

Historically, most experiments used horn antennas to couple power onto bolometers. However, modern Antenna-coupled bolometers integrate the bolometers with a lithographed on-chip antenna through planar transmission lines^{8,9}. These have been successfully deployed in Polarbear¹⁰ and BICEP2,¹¹ and several others will use them over the next decade.

These devices can also contain additional electronics within the transmission lines to process the high-frequency signals prior to down-conversion in the bolometers. For example, the aforementioned experiments integrate band-defining filters into their microstrip lines^{8,9} and others have proposed integrating MEMS switches into the lines to rapidly chop on chip.¹² Another possibility is to fabricate a planar ultra-broadband antenna and couple the received power to bolometers through a channelizer circuit that partitions the bandwidth into narrow channels positioned around the atmospheric lines.¹³ This has already been demonstrated for sub-millimeter observations with Democam, which uses single-polarized pixels, each with 3 colors and it will also be used in MUSIC, with 4 colors per pixel.¹⁴ Multichroic pixels could also facilitate CMB polarimetry, with the added requirement that they be dual-polarized with tightly controlled beam patterns.¹⁵

Experiments with several mapping bands but *monochromatic* pixels will necessarily reflect away out-of-band photons while multichroic pixels can, in principle, receive all of the photons of interest. This can increase the throughput and hence mapping speed by effectively overlapping pixels from different bands, using the focal-plane real-estate more efficiently. Alternatively, for an experiment with a fixed target mapping-speed, a focal plane array of multichroic pixels could significantly reduce the size of the telescope. For satellite missions, where the mission cost is proportional to payload weight, this increase in detector density could provide crucial savings.

We have fabricated a prototype multichroic pixel and we summarize its design in the second section. In the third section, we discuss simulation techniques that facilitated this design and in the fourth, we discuss how we fabricated the devices. We characterized the pixel properties in a simple cryogenic test bed which we describe in the fifth section and we summarize the results of those tests in the sixth. In the concluding section, we describe remaining challenges as well as future directions of this work.

2. PIXEL DESIGN

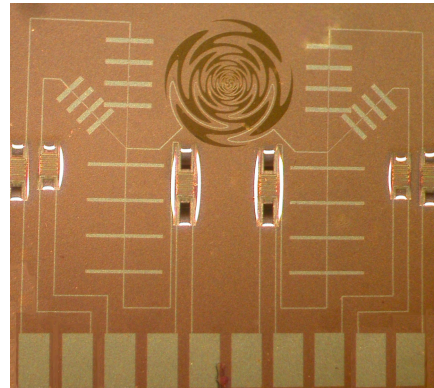


Figure 1. Sinuous Antenna with triplexer circuits on each polarization. The released bolometers are the shiny “H” structures and the spiral antenna’s outer diameter is $1200\text{ }\mu\text{m}$

Figure 1 shows our prototype pixel. Power couples to the on-chip electronics through a sinuous antenna, the four-armed spiral structure in the picture. The sinuous is dual polarized, simultaneously receiving both orthogonal linear polarizations in pairs of opposite arms driven with a 180° phase shift. The bandwidth of an antenna in free space can be arbitrarily wide, limited only by the inner and outer terminations that fix the upper and lower band edges. This antenna has an inner radius of $60\text{ }\mu\text{m}$ and outer of $600\text{ }\mu\text{m}$, providing a continuous bandwidth of 60GHz to 270GHz. The antenna has such a wide band because it is self-similar: ignoring the terminations, the antenna is invariant under a scaling of 69%, which means properties such as impedance and patterns repeat with similar scaling in frequency. The sinuous is an example of a larger class of antennas known

as log-periodics whose properties are invariant when the logarithm of frequency is changed by multiples of an additive factor.¹⁶

The sinuous antenna has a strong heritage in defense industry applications such as RADAR and direction finding. However, we have made two novel modifications to make it appropriate for CMB detection. First, we have placed it on an extended hemispherical contacting lens, picking the extension length to make a synthesized ellipse. This lens refractively and diffractively focuses the natively 60° wide (HPHW) beam so we can match to the f/# of a typical telescope. We used 13.7mm diameter silicon lenses on some of our test pixels (Figure 2(b)), 14mm sintered alumina on others (Figure 2(a)). In both cases, we chose the lens extensions to form a synthesized ellipse. Additionally, the high-permittivity of the lens material suppresses the back-lobe to only 9%, further increasing the gain.¹⁵ The behavior of the sinuous under an antenna has been independently verified by other researchers as well.¹⁷

For the second modification, we replaced the traditional coaxial feed-lines normal to the antenna plane with integrated microstrip transmission lines that use the antenna arms as their ground. This provides a planar structure that we can realize in thin films, as discussed in section 4. These can be seen in Figure 2.

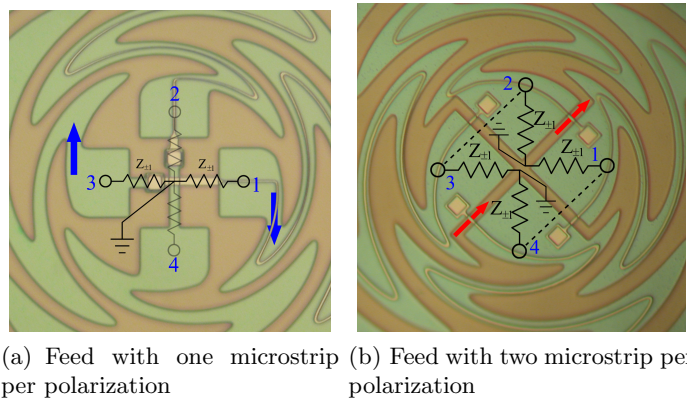


Figure 2. Alternative Microstrip feeds in the antenna interiors. We have superposed the equivalent circuits on the pictures and show the direction of currents, blue for electric and red for magnetic. Each arm has an impedance of $Z_{\pm 1} = 52\Omega$ with respect to virtual ground at center, providing an input impedance of 104Ω .

We have explored two feeding schemes. One scheme drives opposite arms with equal power and opposite phase by shorting a microstrip line from one arm to the opposite (Figure 2(a)). The gradually decreasing width of the ground plane should ensure a balance feed at the center and closely resembles a Dyson Balun.¹⁸ Researchers have used similar feeds with microstrips on two-armed arithmetic spiral antennas.¹⁹ The second scheme feeds each polarization with two microstrips that couple power to slot modes by shorting between adjacent arms (Figure 2(b)). In the first scheme, each polarization leaves the antenna on a single transmission line and can be subsequently channelized before the bolometers. In the second scheme, a hybrid must be used to establish the required phasing between arms, but initial investigations suggest that it has more desirable beams patterns.

Deschamps' formula gives the impedance of a self-complimentary multi-armed antenna in free space.²⁰ After modifying the formula for the approximate impedance on a dielectric half-space, the relevant terms of the impedance matrix are:

$$Z_{\pm 1} \approx \frac{\eta_o/2}{\sqrt{(1 + \epsilon_r)/2}} \frac{1}{\sin^2(\pi/4)} \quad (1)$$

where η_o is the impedance of free space, corrected with the average permittivity of the two sides, ϵ_r corresponding to that of the dielectric.²¹ For silicon, with $\epsilon_r = 11.8$, the impedance of each arm with respect to a virtual ground at center is $Z_{\pm} \approx 52\Omega$, providing a total input impedance of $Z_{in} \approx 104\Omega$. In actuality, simulations show some small reactance of 10Ω which we associate with the antenna being on a dielectric half-space and not hence not truly self-complimentary. Regardless, the thinnest transmission lines that we can fabricate with our

current recipe have a width of $1.5 \mu\text{m}$ and an impedance of 60Ω , which dominates the mismatch and reflects away 7% of the power. In future fabrications, we will modify the recipe for thinner lines and higher impedances.

For the antennas with the dyson-balun feed in Figure 2(a), we partition the bandwidth into multiple channels with either diplexer or Triplexer circuits. These circuits use quarter wavelength shorted-stub filters to remove the different bands, all of which connect to a common node that is fed by the antenna. These circuits are easily visible in Figure 1 to the left and right of the antenna, and the filters in those circuits are currently used by Polarbear and will be used by SPT-pol as well. We connect each filter to the node through transmission lines whose impedance and length ensure that each filters' impedance is infinite (open) in the center of the other filters' pass bands. Beyond the filters, the power terminates in lossy transmission line in close thermal contact with a Transition Edge Sensor (TES).

We have not yet coupled the antenna driven with magnetic slot-currents to a channelizer circuit because we are still developing a broad-band balun. Instead, we fabricated several copies of the same antenna but with different single band-defining filters. We only fed one polarization, and each of the two transmission lines feeding that polarization contained its own filter. By differentially feeding a lumped resistive load on the bolometer, we established the desired 180° phasing between the opposite slots and rejected the unwanted even mode.

3. SIMULATIONS

To provide a model to compare measurements against, we simulated the antenna in the Momentum program of Agilent's Advanced Design Suite (ADS).²² ADS Momentum is a method-of-moments program that directly solves for currents in electromagnetic designs. In particular, we simulated fictitious magnetic currents in the slots within the ground plane. This approach inherently presumes a perfectly conducting ground plane and neglects all superconducting effects, but it drastically reduces the number of unknowns the simulator must solve. The ground plane is at the interface of a semi-infinite half space of silicon on the one side, and air on the other. The microstrip lines run down the back side of the ground plane, separated by a 5000 \AA dielectric film with $\epsilon_r=3.9$.

Because of current computer memory limits of 64GB, it is impractical to simulate the antenna with the lens in a 3-dimensional simulator (e.g. Ansoft's HFSS) that directly solves for the fields. Instead, we accounted for the lens surface with a quasi-optical algorithm that has been used in the study of several other planar lens-coupled antennas.²³ This algorithm traces rays to the lens surface and solves for the fields on the exterior by application of Snell's Law. It then accounts for diffraction with a vectorial Kirchoff Diffraction Integral that interferes all the fields on the lens surface. We produced all simulated curves in Figure 4 with this algorithm.

We must account for the kinetic inductance effect in the superconducting Niobium films in the filter manifolds to faithfully produce the correct band centers. We simulated these in Sonnet,²⁴ modeling each metal film of the microstrip as a superconductor with a surface inductance²⁵ of $L_K=\mu_0\lambda\approx0.13pH/\square$, separated by a similar oxide film as in ADS. All microstrip ports in our simulations were de-embedded with $\lambda/10$ long lines.

4. FABRICATION

We fabricated our devices on 0.5mm thick 4-inch diameter Silicon wafers. We etched the antenna slots into a 3000 \AA thick film of sputtered Niobium (Nb), which superconducts when cooled to below its nominal transition temperature of 9.2K. This film also serves as the ground plane for the microstrip transmission lines and filters. 5000 \AA Silicon Dioxide (SiO_2) separate the ground plane from the 6000 \AA Nb upper conductor. We deposit the oxide with Low Pressure Chemical Vapor Deposition (LPCVD) and we chose the monotonically increasing film thicknesses to ensure step coverage when the upper-conductor either shorts to ground through a via or crosses slots etched into the ground plane.

The microwave circuits terminate their power in either lumped resistive loads created by 2 squares of 400 \AA thick Titanium, or in lossy coiled transmission lines made of an Aluminum-Titanium (Al-Ti) bilayer, with 800 \AA Al, 400 \AA Ti. Naturally occurring metal oxide films between metallic layers that are meant to electrically connect will create parasitic resistance that can compromise the device's performance. To combat this, we strip away Niobium oxide with an Argon plasma immediately before each subsequent metal deposition. These microwave terminations are on release islands in close thermal contact with a Transition Edge Sensor (TES).

The TES-Bolometers reside on a 10,000 Å thick film of silicon-rich Low-Stress-Nitride (LSN) deposited prior to the Niobium ground plane. The TES is the same aluminum-titanium bilayer used for the lossy transmission line, where the Titanium proximitizes the Aluminum to tune the total transition temperature to roughly 500mK. The TES connects to the bias-circuit and SQUID readout through Nb bias lines fashioned out of the same 6000Å film used for the upper microstrip conductors. Finally, we etch the LSN with a fluorine plasma (CF_4) and then release the bolometers with a Xenon-diflouride (XeF_2) etch that locally removes the silicon from under the nitride.

5. TESTBED

We cooled our prototype pixels for testing in an IR-labs dewar shown in Figure 3. We drop our cold-stage to a temperature of 1.2K with pumped liquid helium (^4He) that is buffered from room temperature by a 77K liquid nitrogen (LN_2) stage. The cold-stage is further cooled to 0.24-0.25K with a home-made closed-cycle pumped ^3He fridge.

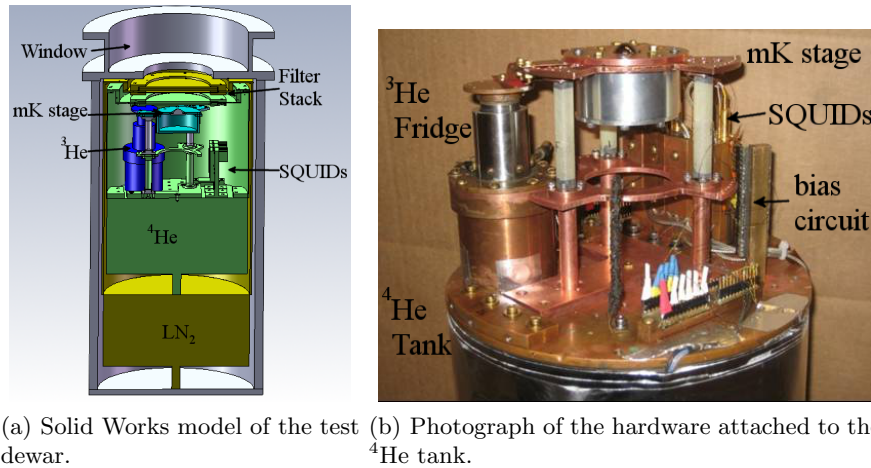


Figure 3. Test dewar used for these measurements

The dewar opens to the room through a 2 inch thick, 4 inch diameter zote-foam window. This material is well known to be 99% transparent to millimeter radiation, but holds a high-vacuum as well. We used 0.12 inches of porous Teflon (porex) as an IR blocker strapped to a window in the 77K radiation shield. We used a metal-mesh 18 cm^{-1} low pass filter at 77K, as well as 14 cm^{-1} and 12 cm^{-1} at 1.2K, all to further reduce high-frequency loading on the cold stage and detectors. Finally, several of the detectors saturated when looking at 300K, so we provided additional shading with 0.25 inch thick MF110 from Emerson-Cuming. We calibrated the loss in this material by repeating many measurements with 0.5 inches of the same material and taking the ratio of throughputs in both cases. The material appears to have losses summarized in Table 1.

Table 1. Optical Power Transmission through MF110

f_{center}	Fractional Transmission
90	55%
150	29%
220	11%

All cited throughput figures include loss in the filters and window, but exclude loss from this attenuator since we are trying to characterize the detector properties in a cryogenic system similar the Polarbear cameras where we plan to deploy them.

The millikelvin stage itself surrounds the backside of the chip with a blackened metal can that terminates the back lobe and only allows the front-lobe through the lens to see through the window. The room temperature window limits the test pixel's field of view to be 88° , which is plenty large to map the beams and side-lobes.

We provided DC bias for our detectors with four 1.5V batteries in series, divided the voltage between a warm $2k\Omega$ and a millikelvin $20\text{ m}\Omega$ resistor in parallel with the bolometer, and varied the final bias voltage across the TES by $10\text{-}100\text{ }\mu\text{V}$ with a room temperature pot. We wired each bolometer in series with the input coil of a SQUID from Quantum Design. However, the inductance of those coils is $2\text{ }\mu\text{H}$, providing an electrical time-constant of $100\text{ }\mu\text{s}$. We have measured the bolometer thermal time-constants in transition to be as low as $10\text{ }\mu\text{s}$, so we had to install a superconducting transformer between the bolometer and SQUID input coil to decrease the electrical time constant and ensure stability.

We characterized the spectral response of our devices with a Fourier Transform Spectrometer. The spectrometer uses a high-pressure mercury-vapor arc lamp (HPK 125W) from Heraeus Noblelight as a source and columnates the beam with a parabolic mirror. Additionally, the instrument uses a 0.01 inch thick film of mylar as a beam splitter between the fixed and variable length arms. Finally, we couple the radiation from the spectrometer to the dewar with light-pipe and use a TPX lens to focus onto our detectors. We convert measured interferograms into spectra with a digital fast-fourier-transform algorithm, and then normalize the peak transmission power to the measured power received by a chopped beam-filling 300-77K load. We also characterized the spectra response of the fourier transform itself by measurements with a broadband bolometer of known properties. All spectra shown in Figure 5 have been divided by this reference spectrum to control for the optics' throughput.

The angular sensitivity in the beam patters is also important, and we measured this with a 0.5 inch diameter chopped nitrogen load on a pair of linear translation stages below the dewar window. We kept the aperture roughly 10 inches below the detector at boresight. In addition to measuring beam patterns, we can also place the source on boresight and rotate a wire polarizing grid between the thermal source and the dewar window to determine cross-polarized leakage.

6. OPTICAL TESTS

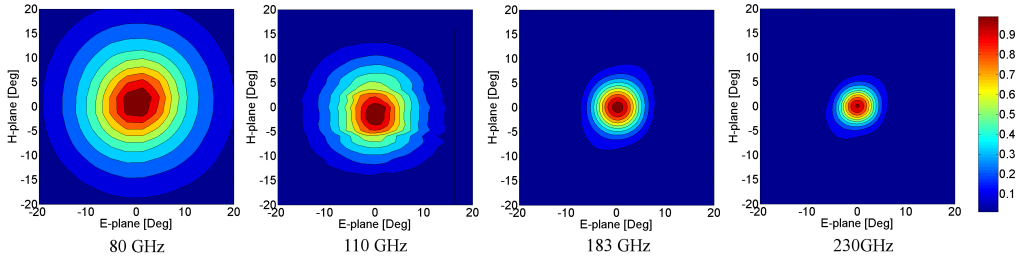
We used the testbed describe above to map beams from the antennas fed in with the magnetic slot-feed (Figure 2(b)). Figure 4 shows the results of these measurements of one polarization as well simulations for comparison. Ellipticity is the difference in the elliptical axes divided by the sum, and the ellipticity for these beams at the half-power contour is no larger than 2.8%. Elliptical beams can systematically leak intensity power into polarization in CMB maps, so this low ellipticity is an important and desirable characteristic of this antenna. In fact, several B-mode search experiments that will soon deploy have similar ellipticities and expect to constrain the tensor-scalar ratio to a level of $r=0.1$.

We have also characterized the devices fed with one microstrip per polarization (Figure 2(a)) but multiple channels per device. Figures 5(a) and 5(b) show the Diplexer and Triplexer spectra. For reference, we have also co-plotted CSO simulations of the atmospheric transmission at Polarbear's current and future cites in Cedar flats and Atacama. The horizontal lines show the designed half-power band-edges as simulated in Sonnet.

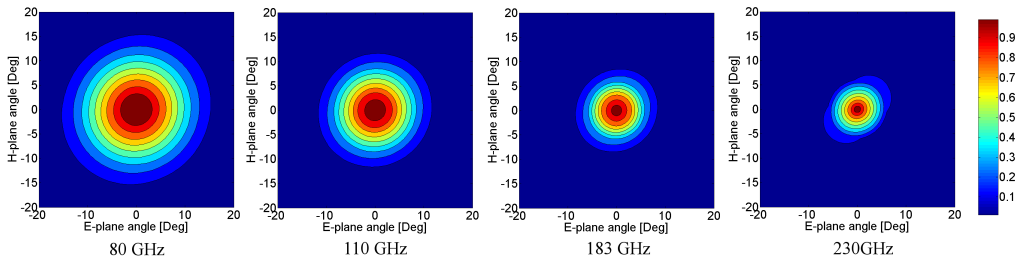
The measured pass bands have averaged throughputs between 18% and 49%, that decrease monotonically with frequency and are clearly located at the correct positions with the designed widths. Recal that these spectra include loss from the filter stack, but exclude the attenuations from the MF110 attenuator. We designed the widths to be conservatively narrow to avoid atmospheric lines, but we can widen these in future re-designs. Due to a design error, one of the 150GHz devices in the triplexer was open and couple not be read.

Figure 6 plots the power transmitted in each Triplexer channel against the orientation of a polarizing grid between the dewar window and chopped source on boresight. As expected, the opposite polarization channels peak 90° out of phase and the power drops to no more than 3% when the grid is crossed. We attribute part of this leakage (1-2%) to the grid itself, and part (1%) to the well known polarization wobble that all planar log-periodic antennas posses. We measured all channels simultaneously, so we suspect that the slight mis-alignment between frequencies is also caused by the wobble.

Finally, Figure 7 show the measured beams from one of the polarizations. The low frequency channels look acceptable, but the upper channel (220GHz) are elliptical, with an ellipticity of 10.4%. The pattern measurements shown Figure 4 suggest that a lens-coupled sinuous can produce circular beams and we suspect that the distortions in these patterns arise from an unbalance in the antenna feed. In particular, the ground plane should narrow



(a) Measured Beams



(b) Simulated Beams

Figure 4. Beams from the antenna fed in the D-feed of Figure 2(b). These beams are from separate devices with single band-defining filters of 20-30% bandwidth.

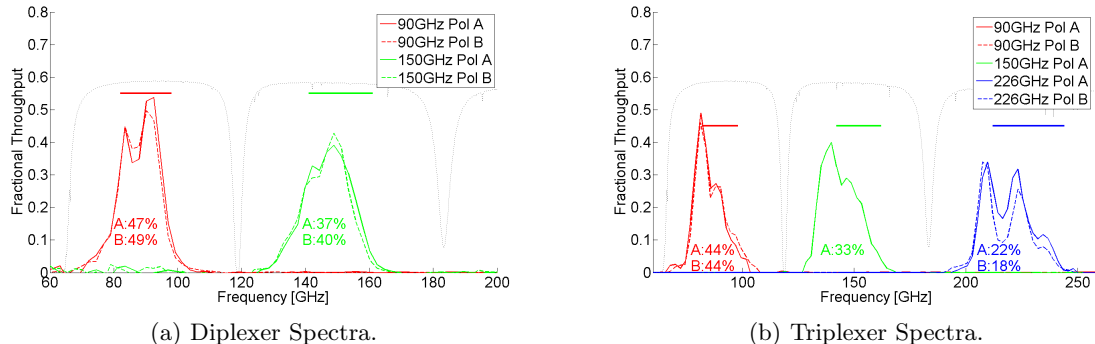


Figure 5. Measured spectra normalized to a chopped load. Horizontal lines show the simulated band-edges and the labels below the graphs report band-averaged throughputs

to the same width as the upper conductor, but we left it several times wider to ease the fabrication. We have already corrected this aspect of the balun in a redesign and have fabricated those devices, but they are currently awaiting optical tests.

7. CONCLUSIONS

The greatest remaining challenge is to feed the antenna in a way that is balanced and can couple to our channelizer circuits. Our current efforts are focused on properly implementing the Dyson-balun feed of Figure 2(a). If this fails, one possibility would be to use the feeds with two microstrips per polarization (Figure 2(b)), channelize each microstrip, and then feed the bolometers differentially. However, this design would require several microstrip crossovers and would require that the our films be uniform over several millimeters to ensure the filters on each microstrip pair are identical.

Alternatively, we could combine each microstrip pair from that feed in a hybrid circuit before channelizing. This alternative is more desirable, but most broadband directional-couplers used for this application must be

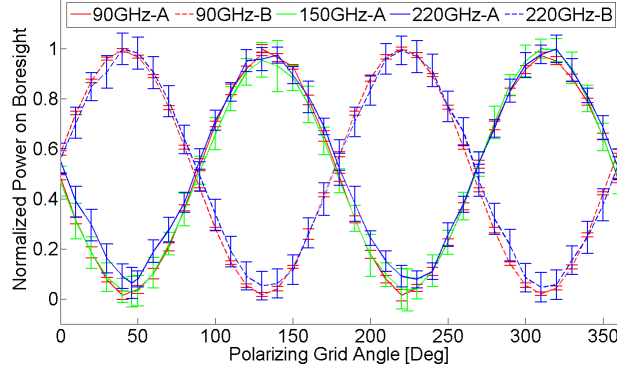


Figure 6. Fraction of Power received from a chopped load on boresight through a polarizing grid.

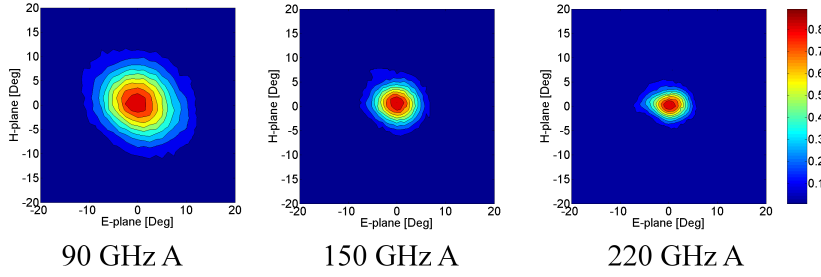


Figure 7. Measured beams from one polarization of the triplexer device. The signal to noise ratio was low because of the optical attenuator and superconducting transformers used.

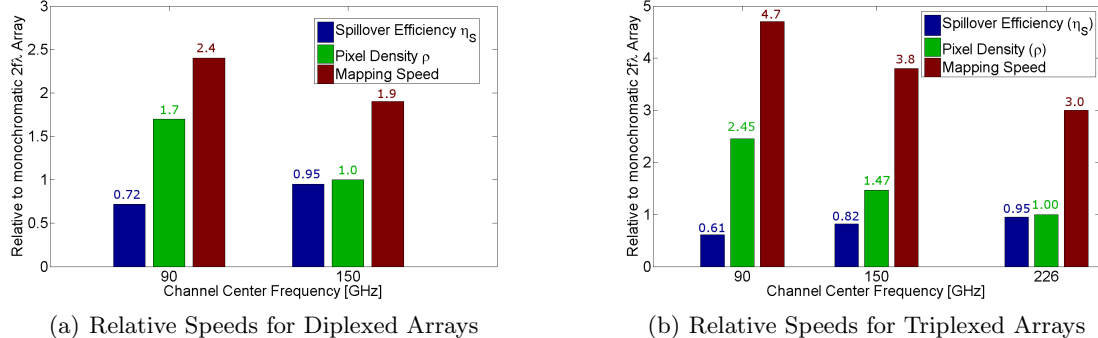
fabricated on dielectric films with a larger thickness per microstrip width than we can achieve with low internal stress. Another hybrid option is to couple the power from each arm onto opposite sides of a coplanar waveguide (CPW), and then couple the CPW to the microstrip input of the channelizer circuits. Simulations suggest that these structures radiate roughly 6% of the power at 220GHz, and we are still working to suppress this further. We have fabricated this device, but have not yet tested it.

Once this feed-balance issue is solved, these pixels could provide a significant boost in mapping speed. A telescope with a focal plane of N pixels with η_S of their power traveling through the aperture should map extended sources (like the CMB) at a speed

$$S \propto \frac{N\eta_S^2}{\eta_S B_{ext} + (1 - \eta_S)B_{int}} \quad (2)$$

where B_{int} and B_{ext} are the internal and external blackbody brightnesses.²⁶ If we upgrade a telescope with channels at 90, 150, and 220GHz but monochromatic pixels to one with the same bands but multichroic triplexed pixels, then the focal plane can contain significantly more detectors. We envision using a camera with a 10K cold stop that terminates the 220GHz beams at the 10% contours. Diffraction on the contacting lens surface forces the lower frequency channels to be wider, increasing the spillover, but those pixels will be denser than the monochromatic arrays, which compensates for the loss. Most importantly, each channel will have three times the number of detectors than the experiment with three monochromatic subarrays, giving a boost of three to the speed. These effects are summarized in Figure 8.

We plan to upgrade the Polarbear camera in a future deployment to include the 90-150 GHz dplexed pixels and expect to boost mapping speeds by a factor of 2 provided that we can actually make a 10K stop. We have also designed, fabricated, and tested a channelizer circuits that contains contiguous bands. This pixel would be appropriate for a satellite mission that does not need to avoid atmospheric lines. This device will be the subject of a future publication.



(a) Relative Speeds for Diplexed Arrays

(b) Relative Speeds for Triplexed Arrays

Figure 8. Diplexed and Triplexer array properties relative to a focal plane with multiple channels each in their own $2f\lambda$ -spaced monochromatic subarrays. Blue shows spillover efficiency where the cold-stop terminates the highest channel at 10%, green shows the relative pixel density, and red shows relative mapping speeds.

ACKNOWLEDGMENTS

This work was supported in part by NASA grant NNG06GJ08G. All devices were fabricated in the Berkeley Microlab at University of California Berkeley's Electrical Engineering Department.

REFERENCES

- [1] Komatsu, E., Smith, K. M., Dunkley, J., Bennett, C. L., Gold, B., Hinshaw, G., Jarosik, N., Larson, D., Nolta, M. R., Page, L., Spergel, D. N., Halpern, M., Hill, R. S., Kogut, A., Limon, M., Meyer, S. S., Odegard, N., Tucker, G. S., Weiland, J. L., Wollack, E., and Wright, E. L., "Seven-Year Wilkinson Microwave Anisotropy Probe (WMAP) Observations: Cosmological Interpretation," *ArXiv e-prints* (Jan. 2010).
- [2] Kaplinghat, M., Knox, L., and Song, Y., "Determining Neutrino Mass from the Cosmic Microwave Background Alone," *Physical Review Letters* **91**, 241301– (Dec. 2003).
- [3] Lyth, D. H., "Introduction to Cosmology," *ArXiv Astrophysics e-prints* (Dec. 1993).
- [4] Mehl, J., Ade, P. A. R., Basu, K., Becker, D., Bender, A., Bertoldi, F., Cho, H. M., Dobbs, M., Halverson, N. W., Holzapfel, W. L., Gusten, R., Kennedy, J., Kneissl, R., Kreysa, E., Lanting, T. M., Lee, A. T., Lueker, M., Menten, K. M., Muders, D., Nord, M., Pacaud, F., Plagge, T., Richards, P. L., Schilke, P., Schwan, D., Spieler, H., Weiss, A., and White, M., "TES Bolometer Array for the APEX-SZ Camera," *Journal of Low Temperature Physics* **151**, 697–702 (May 2008).
- [5] Kogut, A., Dunkley, J., Bennett, C. L., Doré, O., Gold, B., Halpern, M., Hinshaw, G., Jarosik, N., Komatsu, E., Nolta, M. R., Odegard, N., Page, L., Spergel, D. N., Tucker, G. S., Weiland, J. L., Wollack, E., and Wright, E. L., "Three-Year Wilkinson Microwave Anisotropy Probe (WMAP) Observations: Foreground Polarization," *apj* **665**, 355–362 (Aug. 2007).
- [6] Finkbeiner, D. P., Davis, M., and Schlegel, D. J., "Extrapolation of Galactic Dust Emission at 100 Microns to Cosmic Microwave Background Radiation Frequencies Using FIRAS," *apj* **524**, 867–886 (Oct. 1999).
- [7] Benson, B. A., Church, S. E., Ade, P. A. R., Bock, J. J., Ganga, K. M., Hinderks, J. R., Mauskopf, P. D., Philhour, B., Runyan, M. C., and Thompson, K. L., "Peculiar Velocity Limits from Measurements of the Spectrum of the Sunyaev-Zeldovich Effect in Six Clusters of Galaxies," *apj* **592**, 674–691 (Aug. 2003).
- [8] Chattopadhyay, G., Kuo, C.-L., Day, P., Bock, J., Zmuidzinas, J., and Lange, A., "Planar antenna arrays for cmb polarization detection," in [*Infrared and Millimeter Waves, 2007 and the 2007 15th International Conference on Terahertz Electronics. IRMMW-THz. Joint 32nd International Conference on*], 184 –185 (sept. 2007).
- [9] Myers, M. J., Holzapfel, W., Lee, A. T., O'Brient, R., Richards, P. L., Tran, H. T., Ade, P., Engargiola, G., Smith, A., and Spieler, H., "An antenna-coupled bolometer with an integrated microstrip bandpass filter," *Applied Physics Letters* **86**(11), 114103 (2005).

- [10] Lee, A. T., Tran, H., Ade, P., Arnold, K., Borrill, J., Dobbs, M. A., Errard, J., Halverson, N., Holzapfel, W. L., Howard, J., Jaffe, A., Keating, B., Kermish, Z., Linder, E., Miller, N., Myers, M., Niarchou, A., Paar, H., Reichardt, C., Spieler, H., Steinbach, B., Stompor, R., Tucker, C., Quealy, E., Richards, P. L., and Zahn, O., "POLARBEAR: Ultra-high Energy Physics with Measurements of CMB Polarization," in [*American Institute of Physics Conference Series*], H. Kodama & K. Ioka, ed., *American Institute of Physics Conference Series* **1040**, 66–77 (Aug. 2008).
- [11] Orlando, A., Aikin, R. W., Amiri, M., Bock, J. J., Bonetti, J. A., Brevik, J. A., Burger, B., Day, P. K., Filippini, J. P., Golwala, S. R., Halpern, M., Hasselfield, M., Hilton, G., Irwin, K., Jones, W. C., Kenyon, M., Kuo, C. L., Lange, A. E., Leduc, H. G., Mates, B., Morford, T., Nguyen, H. T., Ogburn, R. W., Reintsema, C., Runyan, M., Sudiwala, R., Trangsrud, A., Turner, A. D., and Wilson, P., "Antenna-coupled TES Arrays For The BICEP2/Keck and SPIDER polarimeters," in [*American Institute of Physics Conference Series*], B. Young, B. Cabrera, & A. Miller, ed., *American Institute of Physics Conference Series* **1185**, 471–474 (Dec. 2009).
- [12] Kogut, A., Chuss, D. T., Fixsen, D., Hinshaw, G. F., Limon, M., Moseley, S. H., Phillips, N., Sharp, E., Wollack, E. J., U-Yen, K., Cao, N., Stevenson, T., Hsieh, W., Devlin, M., Dicker, S., Semisch, C., and Irwin, K., "PAPPA: Primordial anisotropy polarization pathfinder array," *New Astronomy Review* **50**, 1009–1014 (Dec. 2006).
- [13] Goldin, A., Bock, J. J., Hunt, C., Lange, A. E., Leduc, H., Vayonakis, A., and Zmuidzinas, J., "SAMBA: Superconducting antenna-coupled, multi-frequency, bolometric array," *Low Temperature Detectors* **605**, 251–254 (Feb. 2002).
- [14] Sayers, J., Czakon, N. G., Day, P. K., Downes, T. P., Duan, R., Gao, J., Glenn, J., Golwala, S., Hollister, M., Leduc, H. G., Mazin, B., Maloney, P. R., Noroozian, O., Nguyen, H. T., Schlaerth, J., Siegel, S., Vaillancourt, J. E., Vayonakis, A., Wilson, P., and Zmuidzinas, J., "Optics for MUSIC: a New (Sub)millimeter Camera for the Caltech Submillimeter Observatory," *these proceedings*.
- [15] O'Brient, R., Edwards, J., Arnold, K., Engargiola, G., Holzapfel, W., Lee, A. T., Myers, M., Quealy, E., Rebeiz, G., Richards, P., Spieler, H., and Tran, H., "Sinuous antennas for cosmic microwave background polarimetry," in [*Society of Photo-Optical Instrumentation Engineers (SPIE) Conference Series*], *Society of Photo-Optical Instrumentation Engineers (SPIE) Conference Series* **7020** (Aug. 2008).
- [16] DuHamel, R., "Dual polarized sinuous antennas." United States Patent 4658262 (1987).
- [17] Liu, L., Xu, H., Percy, R., Herald, D., Lichtenberger, A., Hesler, J., and Weikle, R., "Development of integrated terahertz broadband detectors utilizing superconducting hot-electron bolometers," *Applied Superconductivity, IEEE Transactions on* **19**, 282 –286 (june 2009).
- [18] Dyson, J., "The equiangular spiral antenna," *Antennas and Propagation, IRE Transactions on* **7**, 181 –187 (april 1959).
- [19] Nurnberger, M. and Volakis, J., "A new planar feed for slot spiral antennas," *Antennas and Propagation, IEEE Transactions on* **44**, 130 –131 (jan 1996).
- [20] Deschamps, G., "Impedance properties of complementary multiterminal planar structures," *Antennas and Propagation, IRE Transactions on* **7**, 371 –378 (december 1959).
- [21] Kormanyos, B., Ostliek, P., Bishop, W., Crowe, T., and Rebeiz, G., "A planar wideband 80-200 ghz subharmonic receiver," *Microwave Theory and Techniques, IEEE Transactions on* **41**, 1730 –1737 (oct 1993).
- [22] Agilent, [Advanced Design Suite Momentum v6u2, User Manual], Agilinet (2006).
- [23] Filipovic, D., Gearhart, S., and Rebeiz, G., "Double-slot antennas on extended hemispherical and elliptical silicon dielectric lenses," *Microwave Theory and Techniques, IEEE Transactions on* **41**, 1738 –1749 (oct 1993).
- [24] Corp, S., [Sonnet User manual v. 12.52], Sonnet (2009).
- [25] Kerr, A., "Surface impedance of superconductors and normal conductors in em simulators," Internal Technical Memo Alma Memo No. 245, National Radio Astronomy Observatory, Green Bank, W. Va, USA (1999).
- [26] Griffin, M. J., Bock, J. J., and Gear, W. K., "Relative performance of filled and feedhorn-coupled focal-plane architectures," *Appl. Opt.* **41**(31), 6543–6554 (2002).